Solid Freeform Fabrication 2019: Proceedings of the 30th Annual International Solid Freeform Fabrication Symposium – An Additive Manufacturing Conference
Reviewed Paper

Porosity analysis and pore tracking of metal AM tensile specimen by Micro-CT

Santosh K. Rauniyar, Kevin Chou

Department of Industrial Engineering, University of Louisville, KY 40292

Abstract

In this study, the porosity of Ti-6Al-4V (Ti64) tensile specimen fabricated by laser powder bed fusion (L-PBF) with varying three process conditions was investigated. The variation included the energy density in fabrication (3 levels), the build location (3 levels) and the build orientation (2 levels) for a constant scan speed of 600 mm/s. The tensile specimens were scanned using a micro-CT system before and after tensile testing. The porosity of the specimens varied significantly according to the energy density and the build direction, but only a minor effect of the location change was observed. The fractured specimens showed a significant increase, more than nine percent increase in the pore volume in all cases, for the pore volume as well as the porosity percentage. Also, few large pores were tracked in some of the fractured samples and compared with the as-built counterpart to observe the change in pore morphology.

Keywords: Laser powder bed fusion, Ti64 alloy, Porosity, Computed tomography (CT)

1. Introduction

Material porosity is inherent in the parts manufactured by L-PBF process. It is desirable for some biomedical implants but undesirable for aerospace and automotive components as porosity can lead to unexpected failure [1]. It is necessary to understand the effect of process parameters on the pores, which in turn will allow the user to control the porosity to some extent in the built parts. Multiple techniques have been used by researchers to evaluate the porosity. The most common approach, which is destructive to the specimen, is to cut the specimens and observe the polished cross-sections [2]. A non-destructive technique to characterize the porosity is by using computed tomography [3].

X-ray computed tomography (XCT) can be utilized to obtain a complete three-dimensional structure of a sample with the help of high-resolution scanned images. Though primarily used in the field of life sciences and art conservation, its use in the field of engineering and material science has increased in recent years [4]. Improvement in the pixel size resolution and quicker reconstruction time has led to an increase in the availability as well as the use of XCT [5].

Thompson et al. [6] trace back the use of XCT in additive manufacturing (AM) to 1990 and categorizes the subsequent years in four different timelines. Their review states that from 2010 onwards the use of XCT as an inspection and dimensional measurement tool has increased significantly in the field of AM. Recently, it has also been used by several researchers to detect any internal defects, visualize pore distribution in the samples as well as to analyze the morphometry of pores. However, the accuracy of the results from XCT is highly dependent on the pixel resolution of the scan. Leuders et al [7] used HIP processing to reduce the pore size of Ti64 samples and showed a relative density of 100%

for a scan of 22 μm resolution. Spierings et al [8] compared different density measurement techniques for metallic AM parts and found the result from XCT method as satisfactory. Wits et al [9] concluded in their study that the CT predicts systematically higher relative density due to several reasons, but the CT results are comparable with results from the Archimedes method along with the added capability of investigating pore morphology. Siddique et al [10] showed that there was no significant difference in the result for critical pores obtained from metallographic study and CT scan of voxel resolution of 4.8 μm for AlSi12 samples. Maskery et al [11] concluded that the statistical quality obtained by the data from CT would not be achievable by conventional cross-sectioning and microscopy due to the requirement of a large number of micrographs for their study of 5 mm cube AlSi10Mg samples. Duplesis et al. [12] emphasized on the use of CT for quality control in AM in a series of papers describing a standard method for porosity analysis.

Porosity is one of the common defects in the L-PBF produced parts. It leads to poor density and has an impact on the mechanical properties of the built part [13]. The porosity in the built parts is due to the lack of fusion, keyholing or trapped gas [14]. This study is focused on the analysis of keyhole pores. Keyhole pores are formed when excess energy is imparted to the melt pool by the laser source. In a recent study, Martin et al [15] presented a mitigation strategy to prevent the formation of keyhole pores at the laser turn points.

2. Methodology

The tensile test specimen design is based on standard test methods for tension testing of metallic materials ASTM E8 [16]. The original dimension has been scaled by approximately 50% to reduce the build time. The sample is designed to have a gripping width of 10 mm and is 3 mm thick. Eighteen unique samples were built at different locations and in different orientations with a change in energy density. The scan speed is kept constant at 600 mm/s, and the laser power is varied at 85 W, 100W and 150 W. The combination of scan speed and the power is labeled as low, medium and high for this study. The samples were built with Ti64 powder supplied by LPW technology in an EOSINT M 270 system. Layer thickness and hatch spacing were fixed to 30 μm and 100 μm respectively. The parameters are presented in Table 1. Additionally, the specimens were built at three different locations; location A- closer to the chamber window, location B- on the opposite end of the chamber window and location C- at a height of 35 mm from the build plate on the opposite end of the chamber window. The samples were built in an orientation of 45° (slant-build) and 90° (vertical-build). Three replicates were built for each sample in the same build. Although tensile testing was done for all three sets of replicates, CT scan was done on only one replicate set i.e., replicate set 3. Further details and diagrams of this experiment are presented in a study by Shanshan et al. [17].

Table 1. Experimental parameters for tensile samples

Parameters	Levels	Values
Location	3	A, B, C
Power (Watt)	3	85(L), 100 (M), 150 (H)
Scan speed		600 mm/s
Orientation	2	Slant (S), Vertical (V)

Computed tomography involves taking x-ray projection images of a sample from many angles around the sample. The projection images are taken over a rotation of either 180 or 360 degrees around the sample with small angular increments. These projection images are then mathematically converted into a stack of cross sectional images. The combination of those cross sectional images will generate the three-dimensional volumertic image of the sample.

The CT scanner used in this study is a Bruker micro-CT SkyScan 1173 scanner. The scanner and the zoomed view of the sample with the sample holder inside the scanner are shown in Fig. 1. The scanner is equipped with a 130KV Hamamatsu X-ray source and a 5 MP flat panel sensor camera detector. The x-ray generated from the X-ray source passes through a 0.25 mm thick brass filter, which absorbs the radiation below a certain energy level. An appropriate amount of x-ray transmission is required to obtain a better dynamic image contrast in the scanned images. The low transmission will increase the noise level while the higher transmission will reduce the contrast between different densities in the images. In this study, the transmission was in the range of 20% to 40%.

Fig. 1. Photo of XCT scanner used, zoomed view showing the stage, sample holder and the sample on the sample stage

The sample was put in a sample holder and wrapped around with paraffin tape to restrict any movements of the sample during the scanning process. The sample holder along with the sample was placed on the sample stage and the machine door was closed. During the scan, the sample is rotated with an angular increment of 0.2 degrees from 0 to 360 degrees. One TIF image is generated for each rotation degree totaling to 1800 images from a complete scan. Only the gage portion of the samples was selected for the scan process at a voxel resolution of 6.1 μm. All the scans in this study were completed at 130 KV, 60 μA and exposure time up to 1020 ms.

The projection scan images are converted into 2D cross-sectional grayscale images using reconstruction software. Reconstructed images are saved as 8-bit bitmap image files. During the reconstruction process, the user aims to reduce the artifacts that are inherent to the CT scan process including beam hardening, ring artifact, and misalignment. This process might require user experience to produce the best reconstructed images. Furthermore, pores present in the sample were visualized and the pore morphology was studied using Bruker's analysis software package.

3. Results and Discussion

a) As- built samples scan result

All eighteen samples were scanned at 6.1 µm voxel resolution. Approximately 13.5 mm of the gage length was scanned. Fig. 2 (a) shows a typical sample, (b) shows the preview of the sample in the CT machine and (c) shows the scanned gage region.

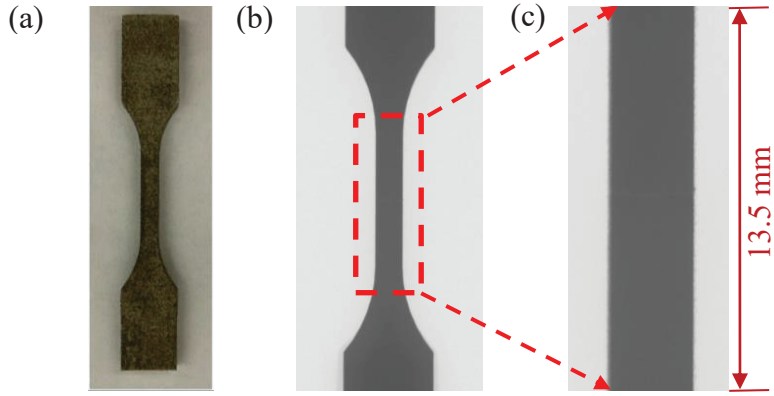

Fig. 2 (a) As-built sample built from L-PBF process; (b) Preview of the sample during the scan and dashed gage region selected to scan; (c) Scanned gage region.

Reconstructed cross-sectional images of the eighteen samples were studied in the data viewer. The results show that there is a relatively large number of pores present in the high energy samples and almost no pores in the medium and low energy samples. The pores are stochastic in nature. A large number of pores existed throughout the entire scanned gage length in the high energy samples while for the medium and low energy case only a few pores could be observed. The typical result of a high, medium and low energy case is shown in Fig. 3 (a), (b), and (c) respectively. The dark black dots represent lower density (pore) and the brighter grey color represents the area with a higher density (solid).

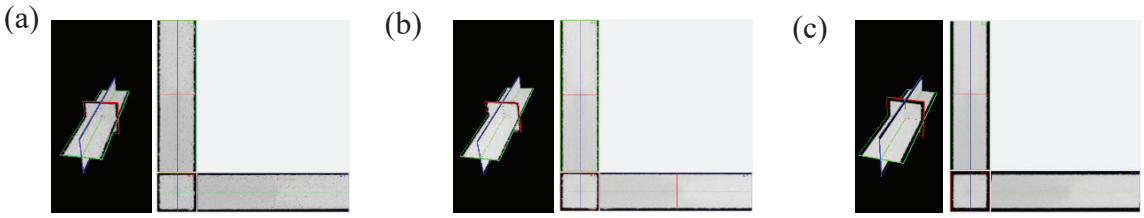

Fig. 3. Typical images result showing three cross-sectional views for (a) high energy (b) medium energy (c) (b) low energy cases

Transverse and Coronal views of all the as-built sample cases are presented in Fig. 4, 5 and 6 below. The samples are coded using alphabets represented the energy density, location, and build orientation respectively. Three identical samples were built for each parameter combination, but only one of the samples from each case was CT scanned. The number after the alphabets represent the sample that was scanned. For example, HAV3 is the code for a high energy sample built at location A and in vertical orientation. The number 3 represents the third set of replicates which was used for CT scan. Among the high energy cases, it is apparent that the location B case has comparatively fewer pores.

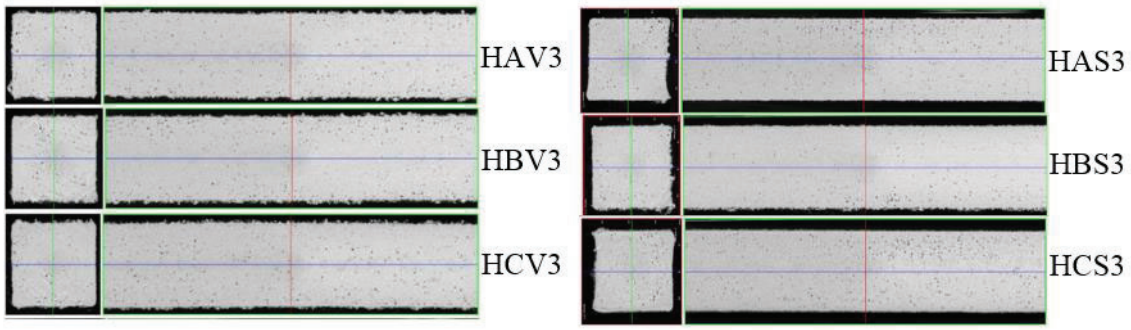

Fig. 4. Transverse and Coronal views of high-level energy density vertical-build specimens (left) and slant-build specimens (right) at different build locations

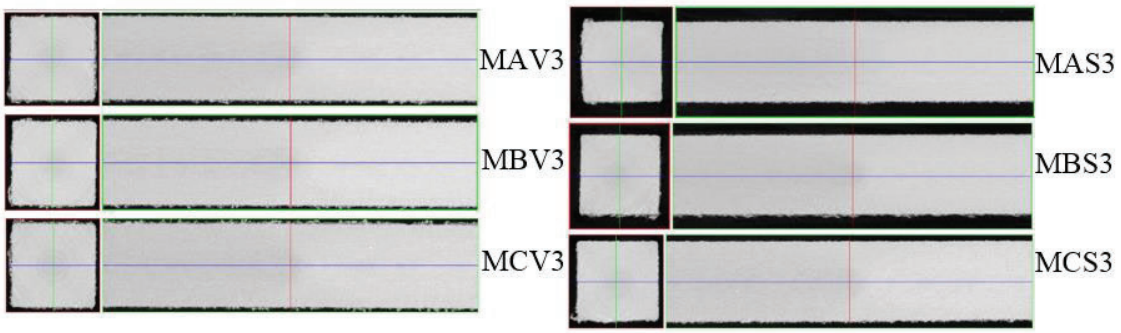

Fig. 5. Transverse and Coronal views of medium-level energy density vertical-build specimens (left) and slant-build specimens (right) at different build locations

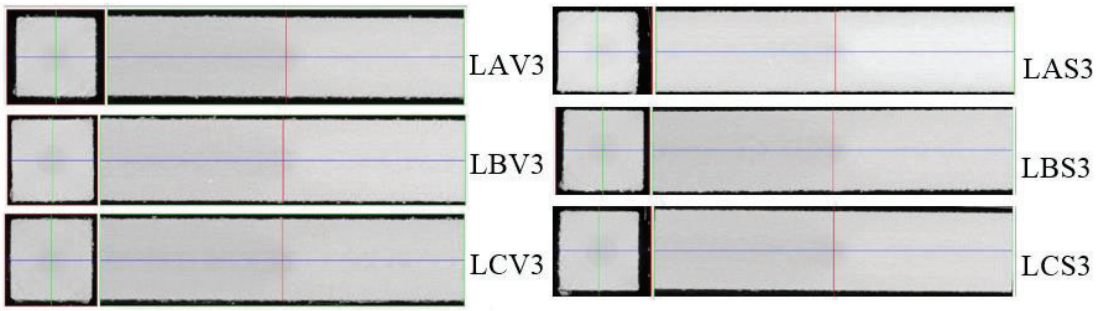

Fig. 6. Transverse and Coronal views of low-level energy density vertical-build specimens (left) and slant-build specimens (right) at different build locations

Visually, almost none or very few pores are observed in the six samples of medium energy level as well as low energy level, as shown in Fig. 8 and 9 respectively.

b) Comparison based on energy level, location, and build orientation

Porosity is analyzed for the entire set of images of all scanned as-built samples. There are approximately 2230 reconstructed cross-sectional image slices in the scanned result of each case. A region of interest is defined, and the image set is converted into binary for further analysis. An example of an image slice and its corresponding binary image is shown in Fig. 7. An average grayscale threshold is applied to all the image slices in the next step.

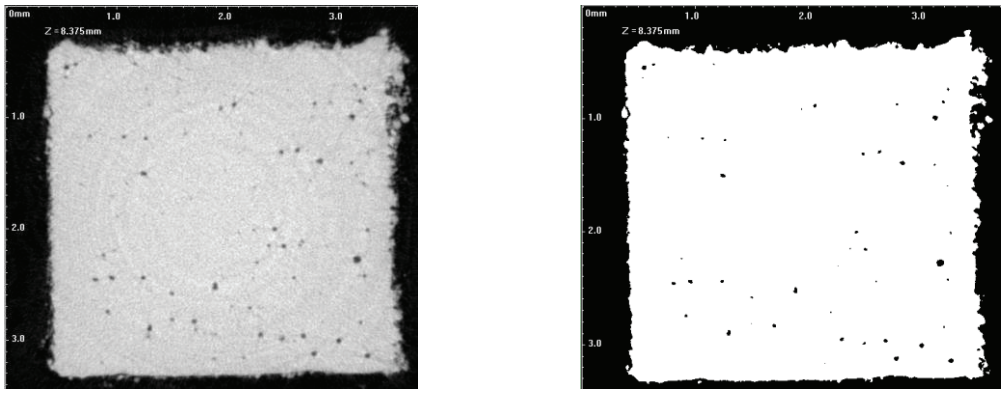

Fig. 7. Example of one image slice and its corresponding binary image

Fig. 8 shows the raw image of one slice and binary images for the same slice for a representative high, medium and low energy case respectively. Only closed pores are considered for porosity analysis. For this analysis, a closed pore in 3D is a connected assemblage of space (black) voxels that is fully surrounded on all sides in 3D by solid (white) voxels. Despeckling of 7 voxels is done in the 3D space to reduce noise before performing porosity analysis.

Fig. 8. Example of one image slice and its corresponding binary image for (a) high (b) medium and (c) low energy cases

The result of 3D pore analysis for all eighteen cases is tabulated below in Table 2 and Table 3. All the results presented in Table 2 are obtained without any despeckling while the results in 3 are obtained after using despeckling function. Despeckling function results in the reduction of the number of pores but no significant reduction in the pore percentage. The use of despeckling function is recommended to remove the small volumes which generally arises due to the image defects in the reconstruction and binarization process rather than the fabrication process itself. So, further analysis and comparison are done considering the analysis result obtained after the use of despeckling function. In this study despeckling of 7 voxels was performed in the entire set of images for porosity analysis. Overall, vertically built samples have a higher number of pores compared to slant-build samples for their corresponding energy level and built location with an exception for high energy sample at Location C. This sample also has the highest pore volume and closed porosity percentage. Pore volume is the total volume of all closed pores and Percentage closed porosity is the volume of closed pores as a percent of the total of solid plus closed pore volume, in the defined location of interest. The slant sample at Location B has the least amount of porosity and pore volume in high-level energy density cases. For medium and low energy density samples, the porosity percentage is less than 2.5×10^{-4}%. And the highest pore volume for medium energy is in the vertically built sample at Location A (7.54×10^{5} μm^3) while for low energy it is in the vertically built sample at Location C ($2.72\times10^{5}\mu m^3$). This part of the study is also presented in a paper by Shanshan et al. [17].

Table 2. Number of pores and porosity percentage (%) in all tensile specimens. (without despeckling)

Orientation	Energy density level	Number of pores in location			Porosity in location		
		A	B	C	A	B	C
Vertical build	High	35846	28815	29006	0.5254	0.3939	0.4592
	Medium	863	806	872	6.7×10-4	3.3×10-4	8.7×10-5
	Low	485	301	528	1×10-4	4.5×10-5	2.6×10-4
Slant build	High	31792	17572	36827	0.4675	0.1917	0.5586
	Medium	680	1156	518	8.7×10-5	3.5×10-4	1.8×10-4
	Low	18	225	596	1.6×10-4	5.4×10-4	1.2×10-3

Table 3. Number of pores and porosity percentage (%) in all tensile specimens. (despeckling of 7 Voxels in 3D)

Orientation	Energy density level	Number of pores in location			Porosity in location		
		A	B	C	A	B	C
Vertical build	High	28225	21946	22540	0.5234	0.3922	0.4576
	Medium	58	72	32	5.9×10-4	2.5×10-4	8.8×10-5
	Low	14	14	20	7.2×10-5	2.3×10-5	2.2×10-4
Slant build	High	24312	13205	24355	0.4656	0.1905	0.5563
	Medium	12	57	30	3.5×10-5	2.6×10-4	1.3×10-4
	Low	12	10	20	1.6×10-4	3.5×10-5	7.4×10-5

c) Relation between tensile properties and the porosity of the samples

A graphical comparison between porosity percentage and ultimate tensile strength (S_{ut}) values of replicate 3 is presented in Fig. 9. There is no clear trend for tensile S_{ut} based on the porosity. But one conclusion can be made is that the slant built high energy samples have the least value of tensile strength among all samples.

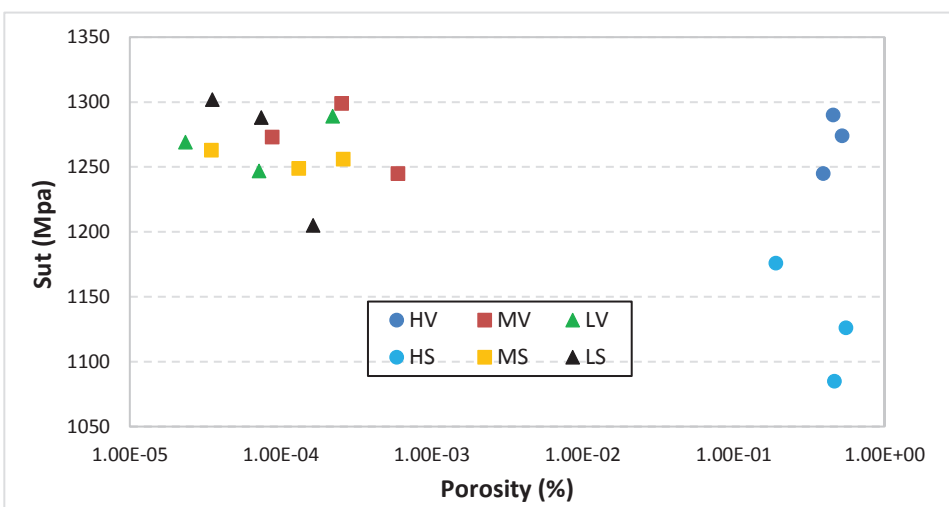

Fig. 9. Graphical representation of S_{ut} of replicate 3 of all sample cases vs. porosity.

d) Fractured samples scan result

After the samples have gone through tensile testing, the fractured samples were scanned again following the same process and similar scan settings as that for the as- built sample which is mentioned in the methodology section. The difference between the scan of the as-built sample and the fractured sample is in the total volume of the sample that will be scanned. As shown in Fig. 10 the two parts of the fractured sample were held together with paraffin tape. But some gap (appx 0.5-1.5mm) is present between those two parts which can be clearly seen in Fig.10(d), This results in a lower scan volume for fractured samples in comparison with their corresponding as-built counterparts. Table 5 presents the number of pores and the porosity percentage for fractured samples. The results show both of those values have increased compared to their as-built counterparts. A detailed comparison is presented in the next section.

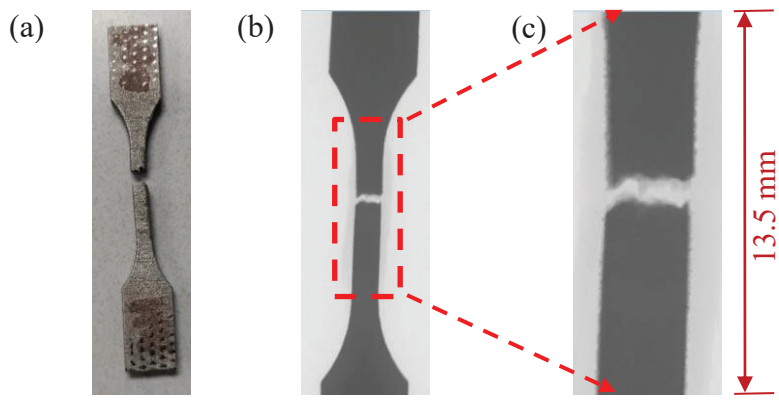

Fig.10. (a) Fractured sample after tensile testing; (b) Preview of the sample during the scan process and dashed region selected to scan; (c) Scanned region.

Table 4. Number of pores and porosity percentage (%) in nine fractured tensile specimens. (despeckling of 7 Voxels in 3D)

Orientation	Energy density level	Number of pores in location			Porosity in location		
		A	B	C	A	B	C
Vertical build	High	30687	23907	24522	0.7525	0.5355	0.5364
	Medium	77	230	28	8.3×10-4	1.3×10-3	1.1×10-4
	Low	230	232	170	1.3×10-3	8.1×10-3	4.4×10-3

e) Porosity comparison between as-built samples and fractured samples

In the next step, the porosity percentage of the as-built sample is compared with the fractured sample. The contrast with this comparison is that the scanned region for the as-built and the fractured samples is not exactly the same. However, the comparison does give a general idea of the change in porosity in the fractured samples. The fractured counterparts of the nine samples that were built in vertical orientation were scanned and compared with the porosity result of their corresponding as-built samples. The details of the porosity comparison for the nine as-built samples and their nine fractured counterparts are presented in Table 5. The volume of the scan region (Volume of interest - VOI) is less for fractured samples because of the gap shown in Fig. 10. Although the VOI has decreased for the fractured samples, porosity percentage has increased significantly as shown in Fig. 11. Overall, the least increase in the pore volume is 9.5 % and the porosity percentage is 17.2 % for the sample FHCV3. FHCV3 represents the fractured sample built with a high energy parameter at location C in a vertical orientation and the number 3 denotes the third replicate. The increase in the pore volume is proportional to the increase in the porosity percentage. Pore tracking shows that there is an increase in the volume of each pore. The approach for the pore tracking and the results obtained is presented in the next section. The medium and low energy samples show a significant percentage increase in their pore volume and there is an overall increase in the number of pores in the fractured samples. It could be the result of the increase in the volume of pores that were earlier not detected by the 6.1 μm resolution of the CT scan in the as-built sample.

Table 5. Porosity comparison (Despeckling @ 7 voxels) of vertically built as-built samples and their fractured counterpart

Samples	Object volume	No. of pores	Pore volume (mm^3)	Porosity
AHV3	126.6	28225	0.67	0.52
FAHV3	114.1	30687	0.87	0.75
	-12.5	2462	29.8%	43.8%
BHV3	127.6	21946	0.50	0.39
FBHV3	113.0	23907	0.61	0.54
	-14.6	1961	21.1%	36.5%
CHV3	125.2	22540	0.58	0.46
FCHV3	116.8	24522	0.63	0.54
	-8.4	1982	9.5%	17.2%
MAV3	126.05	58	7.54E-04	5.98E-04
FMAV3	109.65	77	9.08E-04	8.28E-04
	-16.4	19	20.4%	38.4%
MBV3	126.12	72	3.19E-04	2.53E-04
FMBV3	111.97	230	1.44E-03	1.29E-03
	-14.2	158	352.4%	409.5%
MCV3	126.04	32	1.11E-04	8.77E-05
FMCV3	116.23	28	1.31E-04	1.13E-04
	-9.8	-4	18.5%	28.5%
LAV3	123.67	14	8.88E-05	7.18E-05
FLAV3	107.64	230	1.44E-03	1.29E-03
	-16.0	216	1524.7%	1694.4%
LBV3	123.32	14	2.88E-05	2.33E-05
FLBV3	109.19	232	8.85E-03	8.10E-03
	-14.1	218	30654.4%	34633.5%
LCV3	123.54	20	2.72E-04	2.20E-04
FLCV3	106.58	170	4.66E-03	4.37E-03
	-17.0	150	1612.2%	1884.5%

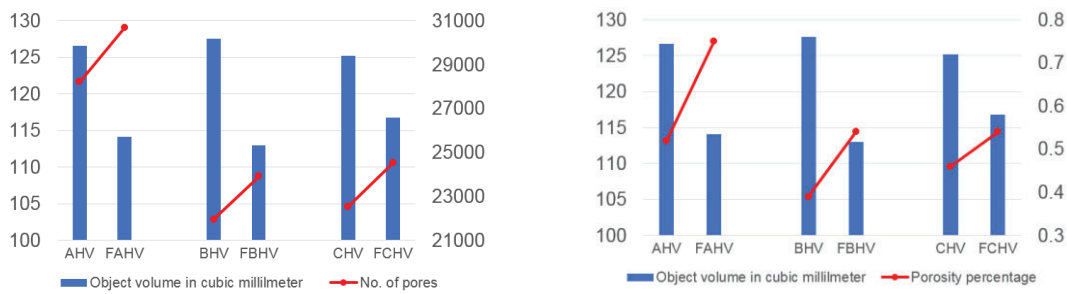

Fig. 11. Graphical comparison of object volume with number of pores (left) and porosity percentage (right) for high energy samples and their fractured counterparts

f) Pore tracking of built and fractured samples

The corresponding as-built sample and the fractured sample image sets were loaded simultaneously in the analysis software and compared side by side based on decreasing order of pore volume. The software generates a list of the pores including the information about pore volume, surface, sphericity, and others. At least 10 pores were tracked for each fractured samples of high energy cases for comparison with their as-built counterparts. Detail comparison of one of the tracked pores is presented in this section. Comparing the pore volume shows that there is an increase in the volume in the fractured samples. One voxel represents a volume of a cube of 6.1 microns. So, one voxel is approximately equal to 227 cubic microns. A comparison between the voxel size and pore diameter of a typical case of HAV and FHAV is presented in Table 6. Pores volume has increased in the fractured sample but the pore with the highest diameter is not present in the fractured sample. Also, the largest pore present in HAV is tracked in FHAV which is the fifth largest pore in FHAV, shown in Fig. 12 and their properties are compared in Table 7. The pore diameter has increased and so does the pore volume.

Table 6. Comparison of volume and pore diameter between HAV and FHAV

	Number of pores	
Voxel size (cubic microns)	HAV	FHAV
0-500	27572	29588
500-1000	578	960
1000-1500	64	110
1500-2000	10	19
2000-2500	1	9
2500-3000	-	1
Total	28225	30687
	Number of pores	
Pore diameter (microns)	HAV	FHAV
10-20	12092	11254
20-30	10570	11556
30-40	4226	5621
40-50	1150	1907
50-60	169	308
60-70	13	33
70-80	3	8
80-90	2	-
Total	28225	30687

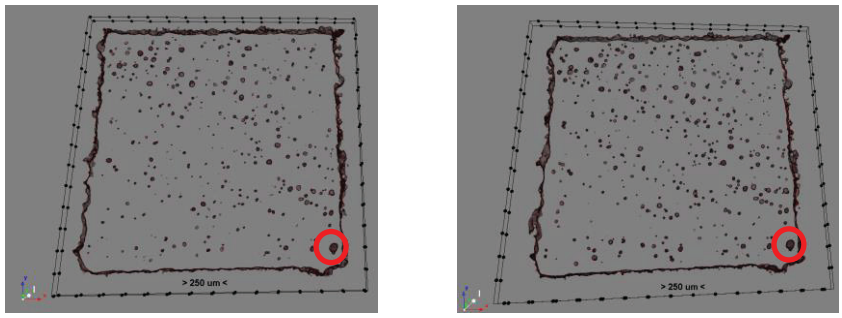

Fig. 12. Approx. 100 micron thickness of the samples, HAV (left image) & FHAV (right image), which have the largest pore in the HAV is compared with the same thickness showing the same pore which is the fifth largest pore in FHAV.

Table 7: Comparison of a pore present in HAV and tracked in FHAV

Sample	Voxel (cubic microns)	Diameter (microns)	Sphericity
HAV	2018	67	0.8067
FHAV	2253	75	0.8148

4. Conclusion

Eighteen tensile samples were scanned using a CT scan system. Reconstruction software was used to generate the cross-sectional images from the projection images. And then the scanned images were visualized using dataviewer software. Porosity analysis was done on the entire image set of all as-built samples. After the scanning process, the tensile test was performed on all samples. Furthermore, scanning, reconstruction, and porosity analysis were carried out for nine fractured samples.

- The number of pores is within 100 and porosity percentage in the range of 10^{-4} for medium and low energy samples.
- From the tensile strength values and porosity percentage comparison, we can say that higher energy density leads to higher porosity in the samples.
- High energy slant-built samples have much lower tensile strength values compared to the vertically built samples. This means the build orientation has a significant effect on the porosity as well as the tensile strength.
- However, there is no clear trend in tensile strength values based on the variation in location.
- There is a significant increase in the pore volume and porosity percentage in fractured samples.
- Pore tracking of individual pores confirms the increase in the volume of pores in fractured samples.

Acknowledgment

This study is supported by the Navy STTR Program, contract No. 18-009 N68335-18-C0371.

References

1. Slotwinski, J. A., Garboczi, E. J. & Hebenstreit, K. M. Porosity Measurements and Analysis for Metal Additive Manufacturing Process Control. 119, (2014). DOI: 10.6028/jres.119.019
2. Dilip, J. J. S. *et al.* Influence of processing parameters on the evolution of melt pool, porosity, and microstructures in Ti-6Al-4V alloy parts fabricated by selective laser melting. *Prog. Addit. Manuf.* 2, 157–167 (2017).
3. Kasperovich, G., Haubrich, J., Gussone, J. & Requena, G. Correlation between porosity and processing parameters in TiAl6V4 produced by selective laser melting. *Materials and Design* 105, 160–170 (2016).
4. S.R Stock, N.K Naik, A.P Wilkinson, K.E Kurtis, X-ray microtomography (microCT) of the progression of sulfate attack of cement paste, Cement and Concrete Research, Volume 32, Issue 10, 1673-1675, (2002)
5. Maire, E. & Withers, P. J. Quantitative X-ray tomography. *Int. Mater. Rev.* 59, 1–43 (2013). Thompson, A., Maskery, I. & Leach, R. K. X-ray computed tomography for additive manufacturing: A review. Meas. Sci. Technol. 27, (2016).
6. Thompson, A., Maskery, I. & Leach, R. K. X-ray computed tomography for additive manufacturing: A review. *Meas. Sci. Technol.* 27, (2016).
7. S. Leuders, M. Thöne, A. Riemer, T. Niendorf, T. Tröster, H.A. Richard, H.J. Maier, On the mechanical behaviour of titanium alloy TiAl6V4 manufactured by selective laser melting: Fatigue resistance and crack growth performance, International Journal of Fatigue, 300-307, (2013)
8. Spierings, A. B., Schneider, M. & Eggenberger, R. Comparison of density measurement techniques for additive manufactured metallic parts. *Rapid Prototyp. J.* 17, 380–386 (2011).
9. Wits, W. W., Carmignato, S., Zanini, F. & Vaneker, T. H. J. Porosity testing methods for the quality assessment of selective laser melted parts. *CIRP Annals - Manufacturing Technology* 65, 201–204 (2016).
10. Siddique, S. *et al.* Computed tomography for characterization of fatigue performance of selective laser melted parts. *Materials and Design* 83, 661–669 (2015).
11. Maskery, I. *et al.* Quantification and characterisation of porosity in selectively laser melted Al-Si10-Mg using X-ray computed tomography. *Materials Characterization* 111, 193–204 (2016).
12. du Plessis, A. & le Roux, S. G. Standardized X-ray tomography testing of additively manufactured parts: A round robin test. *Additive Manufacturing* 24, 125–136 (2018).
13. Gong, H. *et al.* Influence of defects on mechanical properties of Ti-6Al-4V components produced by selective laser melting and electron beam melting. *Materials and Design* 86, 545–554 (2015).
14. Cunningham, R., Narra, S. P., Montgomery, C., Beuth, J. & Rollett, A. D. Synchrotron-Based X-ray Microtomography Characterization of the Effect of Processing Variables on Porosity Formation in Laser Power-Bed Additive Manufacturing of Ti-6Al-4V. *JOM* 69, 479–484 (2017).
15. Martin, A. A. *et al.* Dynamics of pore formation during laser powder bed fusion additive manufacturing. *Nature Communications.* 10, 1–10 (2019).
16. ASTM E8/E8M-11, Standard Test Method for Tension Testing of Metallic Materials. ASTM International, West Conshohocken, PA, 2013.
17. Zhang, S., Rauniyar, S., Shrestha, S., Ward, A. & Chou, K. An experimental study of tensile property variability in selective laser melting. *Journal of Manufacturing Processes* (2019). DOI: 10.1016/j.jmapro.2019.03.045